Hardness and modulus of elasticity of atomic layer deposited Al_2O_3-ZrO_2 nanolaminates and mixtures

Taivo Jõgiaas [a,*], Roberts Zabels [b], Aivar Tarre [a], Aile Tamm [a]

[a] University of Tartu, Institute of Physics, W. Ostwald str. 1, EE-50411, Tartu, Estonia
[b] University of Latvia, Institute of Solid State Physics, Kengaraga str. 8, LV-1063, Riga, Latvia

HIGHLIGHTS

- The hardness's were in the range of 11–15 GPa and moduli 140–180 GPa.
- ZrO_2 alternated or doped with Al_2O_3 layers stabilized mostly in tetragonal phase.
- 3.7 mol.-% of Al was needed to stabilize pure tetragonal ZrO_2.
- The hardness and moduli were insensitive to nanolaminate structure in some cases.

ARTICLE INFO

Keywords:
Atomic layer deposition
Nanoindentation
Nanocomposites

ABSTRACT

Atomic layer deposition was used to produce 90–105 nm thick alumina-zirconia mixtures and nanolaminate structures on soda-lime glass substrate. The resultant chemical and structural compositions of the thin films were characterized. Hardness and modulus of elasticity were determined by instrumented nanoindentation. The hardness of mixtures and nanolaminates were in the range of 11–15 GPa and moduli in the range of 140–180 GPa ZrO_2 with 3.7 mol.-% Al_2O_3 crystallized in pure tetragonal phase and measured hardness reached about 15 GPa on glass substrate at indentation displacement of about 13 nm. Similar mechanical properties were measured in most thin films, except pure ZrO_2, demonstrating insensitivity of mechanical properties to deposition receipt.

1. Introduction

Zirconia is an important material in technology. It has found use in glasses, medical, dental, structural and refractory ceramics, sensors, solid oxide fuel cells, machinery parts and corrosion protection [1–9].

Zirconia is an interesting material due to its several mechanically different crystallographic phases. It exhibits the phase change toughening effect – a metastable tetragonal phase (t-ZrO_2) is induced by deformation stress to convert into monoclinic phase (m-ZrO_2). This results in unit cell volume increase about 3.4%. It requires additional energy to overcome the increment. Therefore, zirconia can withstand mechanical influences at somewhat higher level compared to other oxides. The toughening effect has been used, for instance in powder technology, to enhance properties of other ceramics, including aluminum oxide (zirconia-toughened alumina) [1,10].

In this work, the attention is on atomic layer deposited (ALD) Al_2O_3-ZrO_2 thin films and mixtures thereof, obtained phase composition and related mechanical properties. These composites could be used as mechanically (or chemically) protective coatings, for instance, in micro- or nanoelectromechanical (MEMS/NEMS) devices [11,12]. Due to its nature, ALD can cover all surfaces conformally [13]. So far, the interest in ALD alumina-zirconia has rather considered barrier properties (for instance, encapsulation of electronic devices), electrical or magnetic properties [14–16].

Our previous works on hardness and modulus of ALD HfO_2, Ta_2O_5, Al_2O_3 and ZrO_2 nanolaminates and ALD alumina reinforced SiC nanoparticle compacts have shown high hardness and modulus [17,18]. Compared to our previous results, in this work, the hardnesses and moduli values are considerably higher.

ALD is a bottom-up chemical vapor deposition technique, where successive alternating saturated pulses of vaporized precursors, separated by neutral inert gas pulses (purge pulses), are introduced into a reaction chamber, where in exchange reaction thin films form on solid substrates. This cyclic nature, based on saturated surface reactions, allows deposition of thin films with controlled thicknesses increasing proportionally to the cycle count. Depending on pulsing sequence,

* Corresponding author.
E-mail address: taivo.jogiaas@ut.ee (T. Jõgiaas).

mixtures of materials can be also produced. Therefore, by changing the ratio of deposition cycles of one material to the second, it is possible to tune the composition and structure of deposited thin film.

Usually zirconia is processed at high temperatures (over 1000 °C), but ALD can be conducted at relatively low temperatures. ZrO_2 can be grown at temperature as low as about 200 °C from $ZrCl_4$ and water process [1,2,19]. The content of unwanted impurities (*i. e.* chlorine ions) might have increased levels at low deposition temperatures due to the incomplete surface reactions. Somewhat higher temperatures (300–400 °C for instance) can be used to reduce the levels.

2. Materials and methods

ALD was conducted in a Picosun R200 reactor using deionized water, trimethylaluminum (TMA, 98%, Volatec) and zirconium chloride ($ZrCl_4$, 99.95%, Strem) vapors as precursors. Nitrogen (purity class 5.0) was used as purging/carrier gas. The deposition temperature was 300 °C. $ZrCl_4$ was vaporized at 200 °C and TMA was kept at 19 °C. The deposition substrates were soda lime glass and crystalline silicon Si (100). The pulse sequences were 0.1/4/0.1/10 s (TMA/N_2/H_2O/N_2 respectively) for Al_2O_3 deposition and 0.2/4/1/10 s ($ZrCl_4$/N_2/H_2O/N_2 respectively) for ZrO_2 deposition in the exchange reaction on a substrate. The cycle counts for constituent oxide layer in laminates were derived from depositions of thickest single oxides. The thicknesses of the deposited thin films were in the range of 90–105 nm.

The glass and silicon substrates were cleaned prior depositions with hydrogen peroxide and sulfuric acid mixture (5 min), to remove organic matter from surface, at about 100 °C followed by rinsing with deionized water (5 min) in ultrasonic bath. The silicon substrates were additionally HF-etched (7% solution) for 30 s for removal of the native oxide layer.

The indentations were performed with Agilent Nanoindenter G200 using a Berkovich type diamond indenter in continuous stiffness measurement mode up to 600 nm in depth. To increase the reliability, 10 indentations results were averaged [20–22].

The film thicknesses were measured from Si (100) references using spectroscopic ellipsometry (SE) (Semilab Sopra GES-5E), arms at 75° and wave energies in the range of 1.5–4.5 eV. Fitting was done according to Cauchy model [23].

Crystallographic structure was determined at room temperature using Rigaku SmartLab diffractometer in grazing incidence mode and Cu-Kα radiation. X-ray reflectance (XRR) was used to check and confirm thicknesses and laminated structures of some samples. GlobalFit 2.0 (Rigaku) was used for XRR models.

Thin film elemental compositions were measured with Rigaku ZSX400 X-ray fluorescence spectroscope (XRF). The signal collection times for a characteristic radiation maximum and background were 100 s and a 10 mm diaphragm was used.

3. Results and discussion

3.1. Atomic layer deposition

The deposition recipes, resultant thin film thicknesses and XRF masses per square centimeter are gathered in to Table 1. Densities of thin films are calculated dividing XRF and SE results. There is estimated less than 5% error in XRF measurements of Zr content related to the technical reasons, *i.e.* different substrate position in respect to precursor inlet. (The error for Al is lower.) This also translates to some discrepancy in calculated density values.

The samples can be uniquely identified by their cycle sequences. For example, "$240 \times (2 \times Al_2O_3+3 \times ZrO_2)$" denotes a sequence where 2 cycles of alumina were followed by 3 cycles of zirconia deposition and the double layer sequence was repeated 240 times.

Spectroscopic ellipsometry gives values with about 0.1–0.3 nm error. The possible re-grown sub-layer of SiO_2 on Si (100) references has also been taken into account and it was regularly less than 1 nm. XRR results suggested similar values to SE thicknesses within the accuracy of ±1–2 nm. For instance, the result for sample $37 \times (2 \times Al_2O_3+33 \times ZrO_2)$ was 98.5 nm which compares well with SE derived value of 97 nm. The thicknesses per cycle indicate that for alumina and zirconia the growth was in linear correlation with cycle counts, as is characteristic to ALD.

Table 1
SE thickness results and corresponding thicknesses per cycle (TPC). TPC is thickness of a film divided by the respective cycle counts. XRF results of total material mass per square centimeter is divided by thin film thickness to calculate thin film average density.

Deposition scheme (by cycles)	SE measured thickness, nm	TPC, nm/cyc	Total material mass, μg/cm^2	Density, g/cm^3
$1000 \times Al_2O_3$	92	0.092	26.5	2.9
$500 \times Al_2O_3$	46	0.092	13.4	2.9
$200 \times Al_2O_3$	19	0.095	6.3	3.3
$1300 \times ZrO_2$	104	0.080	64.6	6.2
$650 \times ZrO_2$	53	0.082	34.8	6.6
$270 \times ZrO_2$	22	0.081	13.3	6.0
$240 \times (2 \times Al_2O_3+3 \times ZrO_2)$	96	0.080	47.6	5.0
$64 \times (8 \times Al_2O_3+11 \times ZrO_2)$	91	0.075	48.1	5.3
$20 \times (25 \times Al_2O_3+33 \times ZrO_2)$	93	0.080	48.1	5.2
$36 \times (25 \times Al_2O_3+3 \times ZrO_2)$	89	0.089	29.7	3.3
$37 \times (2 \times Al_2O_3+33 \times ZrO_2)$	97	0.075	61.1	6.3
$14 \times (50 \times Al_2O_3+33 \times ZrO_2)$	97	0.083	41.7	4.3
$5 \times (100 \times Al_2O_3+133 \times ZrO_2)$	94	0.081	45.5	4.8
$6 \times (10 \times Al_2O_3+200 \times ZrO_2)$	97	0.077	61.4	6.3

In XRF measurements, the contents of Al, Zr and O referenced to respective stoichiometric oxides. The measurements of residual elements showed content of Cl to be 0.24% (by weight) at maximum. For carbon, the measured amount was in the range of 2–3%, which seems high, but it is not clear if it is from deposition (*i. e.* from trimethylaluminum precursor) or some contamination from environment.

3.2. Crystallographic structures

The XRD results of pure ZrO_2 samples are depicted in Fig. 1.

The peak indexes for the phases were fitted using Rietveld analysis program Profex (ver. 3.11.1) with single cell parameters of a = 0.361 nm, c = 0.518 nm for the tetragonal phase (PDF 04-005-4207) and a = 0.515 nm, b = 0.521 nm, β = 99.23°, c = 0.532 nm for the monoclinic phase (PDF 04-004-4339) [24]. An approximate analysis indicated presence of $^2/_3$ of monoclinic and $^1/_3$ of tetragonal phase in 104 nm thick ZrO_2 sample. Peak intensities, attributable to the monoclinic phase, upsurge when the thickness increases from 22 nm to 104 nm. This indicates that the relative content of monoclinic phase increases with ZrO_2 layer thickness. Therefore, it is likely that thinner zirconia layers in deposited laminates could be mostly in tetragonal phase. The peak at $2\Theta \approx 47.5°$ in 22 nm thick ZrO_2 pattern goes unexplained as it does not appear in any other patterns nor does it suit to Miller indexing of zirconia phases. It might be related to signal/reflexes from the substrate [25].

In $37 \times (2 \times Al_2O_3+33 \times ZrO_2)$ the reflexes correspond only to tetragonal phase (Fig. 2) with cell parameters of a = 0.358 nm, c = 0.515 nm and density of 6.21 g/cm^3, according to analysis with Profex. Any indication of monoclinic, cubic or orthorhombic phase was not noticed, which suggests the zirconia to be in pure tetragonal phase. The difference in intensity ratios of (101) and (002) reflexes of

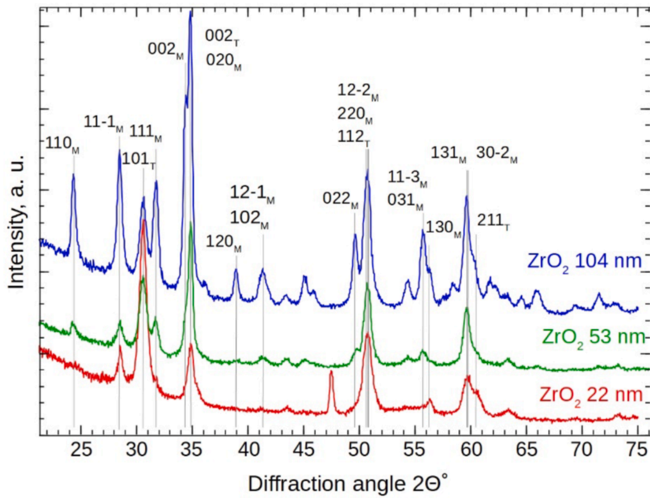

Fig. 1. XRD results of ALD ZrO_2 thin films. M – monoclinic phase; T – tetragonal phase.

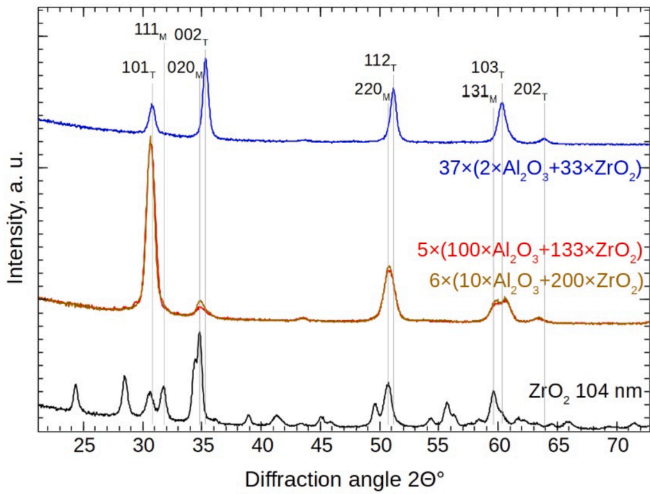

Fig. 2. XRD patterns of crystalline deposited thin films in comparison to ZrO_2.

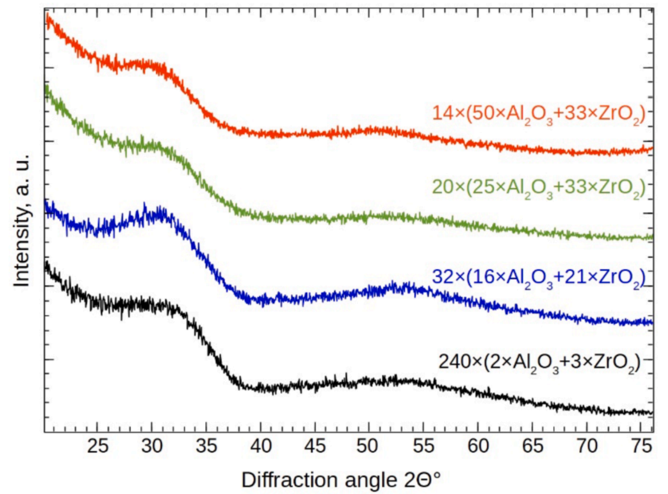

Fig. 3. XRD patterns of nanolaminates with thin layers.

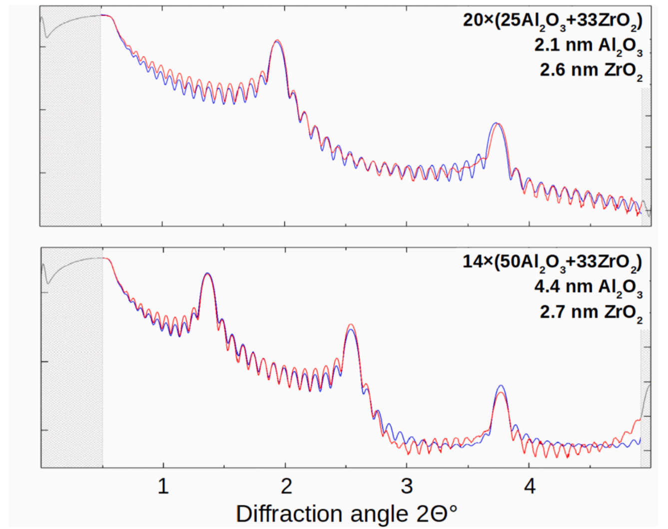

Fig. 4. XRR results and corresponding single layer thicknesses.

sequences $5 \times (100 \times Al_2O_3+133 \times ZrO_2)$ or $6 \times (10 \times Al_2O_3+200 \times ZrO_2)$ compared to $37 \times (2 \times Al_2O_3+33 \times ZrO_2)$, is probably an artefact of texture.

Fig. 2 indicates that ZrO_2 will have high content of tetragonal phase as long as it is alternated or doped with Al_2O_3.

One can note that the XRD patterns are very similar for sequences $5 \times (100 \times Al_2O_3+133 \times ZrO_2)$ and $6 \times (10 \times Al_2O_3+200 \times ZrO_2)$. Alternating ZrO_2 layers with 10 or 100 deposition cycles of Al_2O_3 tends to increase the content of tetragonal phase compared to pure ZrO_2, as can be seen in Fig. 2. Fitting indicated about 90% of t-ZrO_2 for sequences $5 \times (100 \times Al_2O_3+133 \times ZrO_2)$ and $6 \times (10 \times Al_2O_3+200 \times ZrO_2)$, compared to about 30% in 104 nm thick pure zirconia. The presence of other metastable polymorphs like cubic or orthorhombic phases was not confirmed in any sample.

Remaining samples showed no reflexes or had broad peaks (Fig. 3); the crystallographic ordering was markedly reduced. Reflections, which possibly could be correlated to any crystalline alumina, were not noticed [26].

Fig. 4 depicts two XRR measurements of laminated structures. For densities, the best fit for the two examples was found to be 3.0–3.1 g/cm^3 for alumina and 5.8–6.2 g/cm^3 for zirconia. The density of crystalline ZrO_2 corresponds well to literature [27,28]. On the other hand, the given density of Al_2O_3 is remarkably lower compared to crystalline alpha-alumina of 4.0 g/cm^3 [27]. The likely reason is the amorphous nature of the thin film. It has been shown before in XRR measurements that ALD alumina has low density in as deposited state and the density increases during post-deposition annealing [14,29–31]. Compared to previously derived densities from XRF and SE measurements, the XRR results coincide in about 5% margin.

The differences in single layer thicknesses modelled in XRR are off less than 10% compared to expected values calculated from single alumina or zirconia deposition rates and respective cycle count.

3.3. *Elastic moduli and hardnesses*

Although, the total displacement during indentation measurements was up to 600 nm, after 250 nm the results levelled out at substrate property values. Therefore, the results are presented with displacement depths of 300 nm to rather give cleaner look of the graphs at first few hundred nanometers. The substrate level of modulus was around 75 GPa and hardness around 6 GPa.

In Fig. 5 are shown the moduli of thin films with amorphous nature. The graph of sequence $64 \times (8 \times Al_2O_3+11 \times ZrO_2)$ also displays standard deviations (as measured). Overall, the deviations are similar to all

measurements in Fig. 5. The results indicate that the modulus is quite insensitive to cycle or volume ratio of consistent oxides or single layer thickness. Despite the variations, if the crystallographic phase composition could be considered amorphous or near amorphous, the moduli remain similar. This indicates that the elastic properties of the laminates are similar to pure Al_2O_3, which again confirms the zirconia layers to be in harder and stiffer tetragonal phase.

In case of hardnesses (Fig. 6), there were slight differences at displacements of about 40–80 nm, where the thin films of pure alumina and alumina with zirconia doping had hardnesses about 1 GPa higher than the others.

The average hardness for 36 × (25 × Al_2O_3+3 × ZrO_2) seems higher than for pure alumina. This probably could be related to the ≈15% higher density, according to combined XRF and SE measurements. The density for 36 × (25 × Al_2O_3+3 × ZrO_2) was calculated to be approximately 3.4 g/cm^3 compared to 2.9 g/cm^3 for pure Al_2O_3 thin film.

The moduli values for thin films with notable ZrO_2 crystallinity (Fig. 7) were similar to amorphous thin films and to each other. The exception was pure ZrO_2 thin film, which showed increase in modulus after initial drop to minimum at around 50 nm displacement, probably due to pile-up effect during indentation.

In macroscopic scale the hardness of ZrO_2 polymorphs have been 6.6–7.3 GPa for monoclinic, 7–12 GPa for tetragonal and 7–17 GPa for cubic phase, depending on the type of stabilizer element used and its amount [1]. Compared to that, in Fig. 8, the hardness of pure ZrO_2 is in similar range for monoclinic and tetragonal phases, which is in good correlation with the mixed monoclinic/tetragonal phase composition of ALD ZrO_2. The increase in hardness, after its initial drop to minimum near 50 nm of displacement, could be related to material pile-up during indentation [32,33] or phase change of tetragonal ZrO_2 (phase change toughened thin film). The latter could be expected for other thin films showing tetragonal phase, but cannot be noticed in Fig. 8. Therefore, the pile-up phenomena is more likely to cause the hardness increase of ZrO_2 thin film.

In Fig. 8, the hardness of thin film 37 × (2 × Al_2O_3+33 × ZrO_2) drops steeply at first several measurement points. Similar behavior can be seen, if the hardness ratio of thin film to substrate is remarkably different [34]. Fitting the data points to an exponential function indicated that the hardness for sequence 37 × (2 × Al_2O_3+33 × ZrO_2) could be around 16 GPa (at 0 nm of displacement).

The results of hardness, modulus and density values are gathered in Table 2. The values are given at the shallowest indentation displacement of ≈13 nm as averages measured on glass substrate. Due to the measurement discrepancy, ZrO_2 has been omitted from the table.

It can be seen that there is a little difference in hardness and modulus

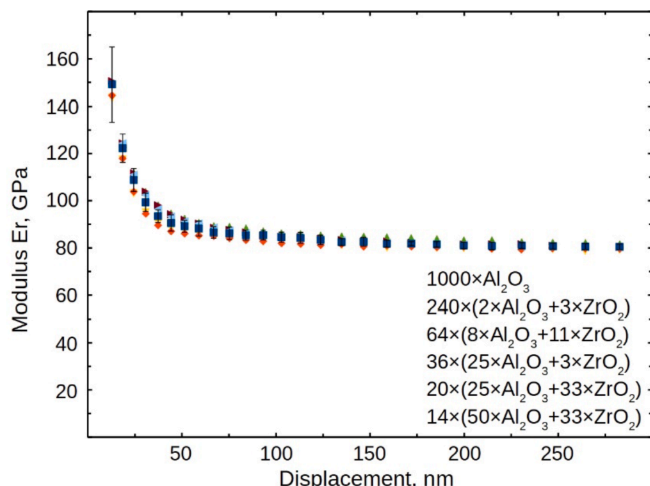

Fig. 5. Reduced moduli of amorphous Al_2O_3-ZrO_2 thin films.

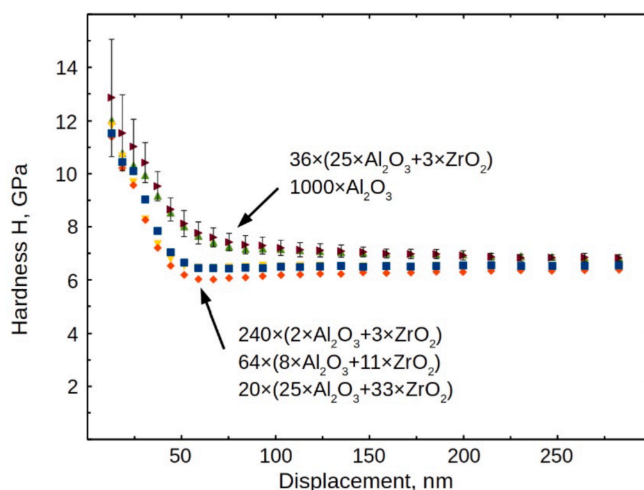

Fig. 6. Hardnesses of amorphous Al_2O_3-ZrO_2 thin films. The 36 × (25 × Al_2O_3+3 × ZrO_2) sequence is noted as top most triangles (pointing right).

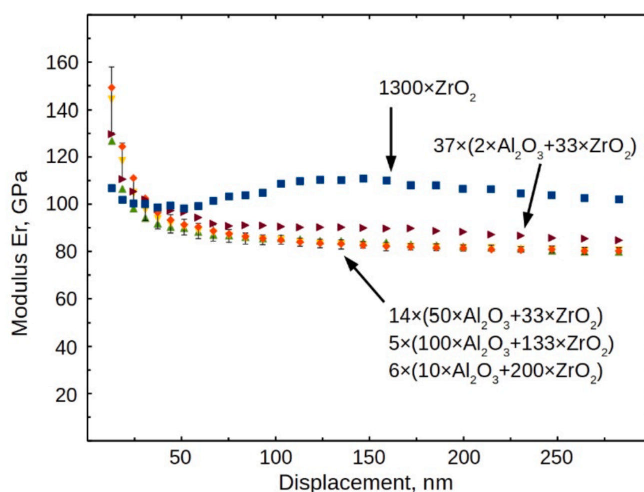

Fig. 7. Moduli of crystalline Al_2O_3-ZrO_2 thin film composites and pure ZrO_2.

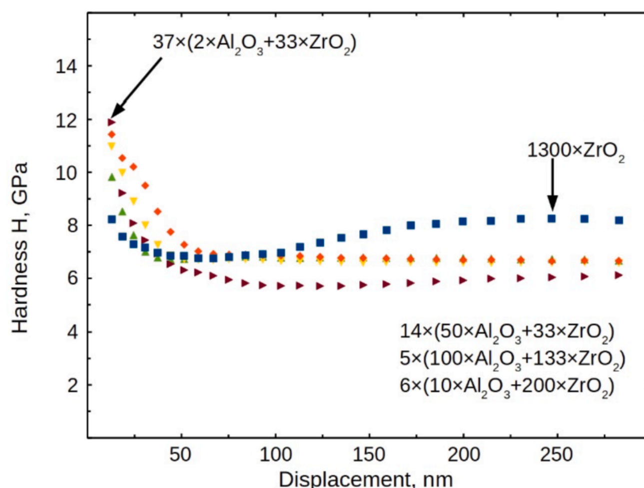

Fig. 8. Hardness values for ALD Al_2O_3-ZrO_2 thin films with crystalline nature.

Table 2
A summary of hardness and modulus values of Al_2O_3-ZrO_2 nanocomposites, mixtures.

Deposition scheme (by cycles)	Measured thickness, nm	TPC, nm/cyc	Hardness, GPa	Modulus, GPa	Density, g/cm^3
$1000 \times Al_2O_3$	92	0.092	12.0	150	2.9
$240 \times (2 \times Al_2O_3+3 \times ZrO_2)$	96	0.080	10.4	144	5.0
$64 \times (8 \times Al_2O_3+11 \times ZrO_2)$	91	0.075	11.5	149	5.3
$20 \times (25 \times Al_2O_3+33 \times ZrO_2)$	93	0.080	11.8	143	5.2
$36 \times (25 \times Al_2O_3+3 \times ZrO_2)$	89	0.089	12.8	150	3.3
$37 \times (2 \times Al_2O_3+33 \times ZrO_2)$	97	0.075	11.9	130	6.3
$14 \times (50 \times Al_2O_3+33 \times ZrO_2)$	97	0.083	12.0	149	4.3
$5 \times (100 \times Al_2O_3+133 \times ZrO_2)$	94	0.081	11.0	144	4.8
$6 \times (10 \times Al_2O_3+200 \times ZrO_2)$	97	0.077	9.8	127	6.3

values for thin film of pure Al_2O_3 and nanolaminate $14 \times (50 \times Al_2O_3+33 \times ZrO_2)$. This is probably because the properties are similar for alumina and tetragonal zirconia, which is likely present in ZrO_2 layers. The same similarity can be observed for other thin films with thinner single layers. There also seems to be a tendency of lower hardness in case of reduced crystallinity in the thin films. Compared to pure Al_2O_3, the higher hardness of $36 \times (25 \times Al_2O_3+3 \times ZrO_2)$ is likely due to increased density of ≈15%.

The results for $6 \times (10 \times Al_2O_3+200 \times ZrO_2)$ are somewhat unsuitable. It is a crystalline film with XRD pattern almost identical to $5 \times (100 \times Al_2O_3+133 \times ZrO_2)$ and has high density (similar to $37 \times (2 \times Al_2O_3+33 \times ZrO_2)$). Yet the hardness and modulus are lower in both cases. Based on the presented data set, the phenomena remains experimentally unexplained, but probable reason could be grain boundary sliding due to very thin Al_2O_3 layer (inverse Hall-Petch effect) [35,36].

Common hard material classes, besides oxides, are carbides and nitrides. Depending on the conditions (substrate temperature, deposition environment pressure *etc.*), composition and used methods, carbides can possess hardnesses from 9 to 35 GPa [37–43]. The higher hardness values are usually obtained at higher temperatures than 300 °C and enable development of harder films (20–35 GPa). In this regard, the deposited ALD thin films showed comparable or even higher values [37–39].

Al_2O_3-ZrO_2 nanolaminates have been produced by other methods. For instance, Portinha et al. have used reactive magnetron sputtering and held deposition substrates at 300 °C as in current work. The single oxide layer thicknesses were 14 nm or below. Their as deposited samples had hardnesses of 15 GPa or below and moduli of 160–180 GPa. It was found that annealing increased hardness at best to 24 GPa and moduli above 200 GPa. They noted that internal compressive stresses in Al_2O_3-ZrO_2 nanolaminate could be the reason [44].

In another work, Ito et al. produced Al_2O_3-ZrO_2 nanocomposites using laser chemical vapor deposition. They found that deposition at 1207 K and 1000 K would result in tetragonal ZrO_2 dendrites grown inside columnar grains of alpha- or gamma-Al_2O_3. The latter had hardness of 28 GPa, comparable to alpha-alumina [45].

Pulsed laser deposition was used by Balakrishnan et al. to obtain ZrO_2/Al_2O_3 nanomultilayers. Hardness values for single oxides were determined to be 20.8 GPa for alumina and 10 GPa for polycrystalline zirconia. The hardnesses for laminates were reported to be around 11–15 GPa. Moduli were reported to be approximately 340 GPa for alumina thin film, 175 GPa for zirconia and around 200 GPa for nanomultilayers [46].

Compared to current work, the main difference with the last referenced publications is that all those thin films consisted crystalline alumina, whereas ALD alumina is amorphous, has lower density and, therefore, reduced hardness and modulus (Table 3).

Physical deposition methods, including sputtering and laser-enhanced techniques, tend to be sensitive to deposition direction (*i. e.* relative positioning of material source and target substrate) and therefore have lower conformity with a substrate. ALD on the other hand has high conformity, including various 3D substrates, which would be preferable in MEMS and NEMS technology [47].

Table 3
Hardness and modulus of elasticity values of some ALD thin films.

Material	Hardness, GPa	Modulus, GPa	Reference
Al_2O_3	7.3–12.3	156–220	[17,48,49,50,51]
ZrO_2	7.0	86	[17]
HfO_2	9.1–14.4	197–220	[11,17]
TiO_2	8.3	151	[48]
ZnO	6.6–8.3	135–154	[26]
Ta_2O_5	6.7	96	[17]
Al_2O_3:ZnO (1:19)	10.6	138	[26]

Table III indicates that the ALD thin films presented in this work, in most cases, have enhanced hardness.

4. Conclusions

Atomic layer deposition of composite structures consisting Al_2O_3 and ZrO_2 can be used to produce hard and stiff thin films. Almost phase-pure tetragonal ZrO_2 can be obtained. The Al_2O_3-ZrO_2 thin films showed high hardness (10–13 GPa) and relatively high modulus (130–150 GPa) as measured on soda-lime-glass substrates. The respective values for thin films, apart from glass substrate, would be higher because the properties of glass were inferior and therefore would reduce the properties of thin films. The hardnesses and moduli were similar to all compositions and quite insensitive to used deposition sequence or resultant crystallographic phase composition. This could be attributed to the similarity in mechanical properties of amorphous alumina and tetragonal zirconia. The content of tetragonal zirconia was increased with the addition of alumina in the composition to the extent of fully tetragonal phase composition in case of 3.7 at.-% of alumina in zirconia. Therefore, if a harder and stiffer crystalline ZrO_2 coating is needed, alumina can be used to stabilize zirconia (mainly) in tetragonal phase. As seen from the indentation results, the mechanical behavior of pure zirconia thin film could be somewhat unpredictable, opposed to smooth behavior of thin films with alumina. Nevertheless, there seems to be some room for improvement in mechanical properties of ALD Al_2O_3 or ZrO_2 or composites thereof.

Declaration of Competing Interest

The authors declare that they have no known competing financial interests or personal relationships that could have appeared to influence the work reported in this paper.

Acknowledgements

This work was funded by the European Regional Development Fund project TK134 “Emerging orders in quantum and nanomaterials”, Estonian Research Agency project PRG4 “Emerging novel phases in strongly frustrated quantum magnets”.

References

[1] R.W. Cahn, P. Haasen, E.J. Kramer, in: M.V. Swain (Ed.), Materials Science and Technology a Comprehensive Treatment: Structure and Properties of Ceramics, vol. 11, VCH, 1994, ISBN 3-527-26813-8.

[2] Zirconia, third ed., Elsevier, 1992, ISBN 978-1-4831-7820-2.

[3] R.W. Cahn, P. Haasen, E.J. Kramer, in: D.F. Williams (Ed.), Materials Science and Technology a Comprehensive Treatment: Medical and Dental Materials, vol. 14, VCH, 1992, ISBN 3-527-26813-8.

[4] H. Chai, A.J. Mieleszko, S.J. Chu, Y. Zhang, Using glass-graded zirconia to increase delamination growth resistance in porcelain/zirconia dental structures, Dent. Mater. 34 (1) (2018), https://doi.org/10.1016/j.dental.2017.11.004.

[5] S. Saremi-Yarahmadi, J. Binner, B. Vaidhyanathan, Erosion and mechanical properties of hydrothermally-resistant nanostructured zirconia components, Ceram. Int. 44 (9) (2018), https://doi.org/10.1016/j.ceramint.2018.03.074.

[6] N. Miura, T. Sato, S.A. Anggraini, H. Ikeda, S. Zhuiykov, A review of mixed-potential type zirconia-based gas sensors, Ionics 20 (7) (2014), https://doi.org/10.1007/s11581-014-1140-1.

[7] F. Heydari, A. Maghsoudipour, Z. Hamnabard, S. Farhangdoust, Mechanical properties and microstructure characterization of zirconia nanoparticles glass composites for SOFC sealant, Mater. Sci. Eng. A 552 (2012), https://doi.org/10.1016/j.msea.2012.05.019.

[8] Y.W. Gu, A.U.J. Yap, P. Cheng, K.A. Khor, Zirconia-glass ionomer cement – a potential substitute for Miracle Mix, Scr. Mater. 52 (2) (2005), https://doi.org/10.1016/j.scriptamat.2004.09.019.

[9] A.M. Kamalan Kirubaharan, P. Kuppusami, R. Priya, R. Divakar, M. Gupta, D. Pandit, S. Ningshen Synthesis, Microstructure and corrosion behavior of compositionally graded Ni-YSZ diffusion barrier coatings on Inconel-690 for applications in high temperature environments, Corros. Sci. 135 (2018), https://doi.org/10.1016/j.corsci.2018.02.053.

[10] M.D. Barros, P.L. Rachadel, M.C. Fredel, R. Janssen, D. Hotza, Mechanical behavior of zirconia-toughened alumina laminate with or without Y-PSZ intermediate layers, J. Ceram. Sci. Technol. 09 (1) (2018), https://doi.org/10.4416/JCST2017-00077.

[11] M. Berdova, X. Liu, C. Weimer, A. Lamperti, G. Tallarida, E. Cianci, M. Fanciulli, S. Franssila, Hardness, elastic modulus, and wear resistance of hafnium oxide-based films grown by atomic layer deposition, J. Vac. Sci. Technol. A: Vac. Surf. Films 34 (2016), 051510, https://doi.org/10.1116/1.4961113.

[12] I.S.Y. Ku, T. Reddyhoff, A.S. Holmes, H.A. Spikes, Wear of silicon surfaces in MEMS, Wear 271 (7–8) (2011), https://doi.org/10.1016/j.wear.2011.04.005.

[13] N.D. Hoivik, J.W. Elam, R.J. Linderman, V.M. Bright, S.M. George, Y.C. Lee, Atomic layer deposited protective coatings for micro-electromechanical systems, Sens. Actuators 103 (2003), https://doi.org/10.1016/S0924-4247(02)00319-9.

[14] M. Broas, O. Kanninen, V. Vuorinen, M. Tilli, M. Paulasto-Kröckel, Chemically stable Atomic-layer-deposited Al_2O_3 films for processability, ACS Omega 2 (2017), https://doi.org/10.1021/acsomega.7b00443.

[15] J. Oh, S. Shin, J. Park, G. Ham, H. Jeon, Characteristics of Al2O3-ZrO2 laminated films deposited by ozone-based atomic layer deposition for organic devaice encapsulation, Thin Solid Films 599 (2016), https://doi.org/10.1016/j.tsf.2015.12.044.

[16] K. Kukli, M. Kemell, H. Castán, S. Dueñas, H. Seemen, M. Rähn, J. Link, R. Stern, M. J. Heikkilä, M. Ritala, M. Leskelä, Atomic layer deposition and performance of ZrO_2-Al_2O_3 thin films, ECS J. Solid State Sci. Technol. 7 (2018), https://doi.org/10.1149/2.0021806jss.

[17] T. Jõgiaas, R. Zabels, A. Tamm, M. Merisalu, I. Hussainova, M. Heikkilä, H. Mändar, K. Kukli, M. Ritala, M. Leskelä, Mechanical properties of aluminum, zirconium, hafnium and tantalum oxides and their nanolaminates grown by atomic layer deposition, Surf. Coat. Technol. 282 (2015), https://doi.org/10.1016/j.surfcoat.2015.10.008.

[18] T. Jõgiaas, L. Kollo, J. Kozlova, A. Tamm, I. Hussainova, K. Kukli, Effect of atomic layer deposited aluminium oxide on mechanical properties of porous silicon carbide, Ceram. Int. 41 (2015), https://doi.org/10.1016/j.ceramint.2015.02.074.

[19] S. Abbas, S. Maleksaeedi, E. Kolos, A.J. Ruys, Processing and properties of zirconia-toughened alumina prepared by gelcasting, Materials 8 (2005), https://doi.org/10.3390/ma8074344.

[20] M.R. VanLandingham, Review of instrumented indentation, J. Res. Natl. Inst. Stand. Technol. 108 (4) (2003), https://doi.org/10.6028/jres.108.024.

[21] X. Li, B. Bhushan, A review of nanoindentation continuous stiffness measurement technique and its applications, Mater. Char. 48 (2002), https://doi.org/10.1016/S1044-5803(02)00192-4.

[22] W.C. Oliver, G.M. Pharr, Measurement of hardness and elastic modulus by instrumented indentations: advances in understanding and refinements to methodology, J. Mater. Res. 19 (1) (2004), https://doi.org/10.1557/jmr.2004.19.1.3.

[23] H. Fujiwara, Spectroscopic Ellipsometry: Principles and Applications, John Wiley & Sons Ltd, 2007, ISBN 978-0-470-01608-4.

[24] N. Doebelin, R. Kleeberg Profex, A graphical user interface for the Rietveld refinement program BGMN, J. Appl. Crystallogr. 48 (2015), https://doi.org/10.1107/S1600576715014685.

[25] N. Petermann, T. Schneider, J. Stötzel, N. Stein, C. Weise, I. Wlokas, G. Schierning, H. Wiggers, Microwave plasma synthesis of Si/Ge and Si/WSi2 nanoparticles for thermoelectric applications, J. Phys. D Appl. Phys. 48 (2015) 314010, https://doi.org/10.1088/0022-3727/48/31/314010.

[26] T. Homola, V. Buršíková, T.V. Ivanova, P. Souček, P.S. Maydannik, D.C. Cameron, J.M. Lackner, Mechanical properties of atomic layer deposited Al_2O_3/ZnO nanolaminates, Surf. Coat. Technol. 284 (2015), https://doi.org/10.1016/j.surfcoat.2015.07.078.

[27] D.R. Lide (Ed.), CRC Handbook of Chemistry and Physics, 86th Edition, CRC Press, Taylor & Francis Group, LLC, 2005, 10: 0-8493-0486-5, ISBN-13: 978-0-8493-0486-6.

[28] D.M. Hausmann, E. Kim, J. Becker, R.G. Gordon, Atomic layer deposition of hafnium and zirconium oxides using metal amide precursors, Chem. Mater. 14 (10) (2002), https://doi.org/10.1021/cm020357x.

[29] M.D. Groner, F.H. Fabreguette, J.W. Elam, S.M. George, Low-temperature Al_2O_3 atomic layer deposition, Chem. Mater. 16 (2004), https://doi.org/10.1021/cm0304546.

[30] C. Barbos, D. Blanc-Pelissier, A. Fave, C. Botella, P. Regreny, G. Grenet, E. Blanquet, A. Crisci, M. Lemiti, Al_2O_3 thin films deposited by thermal atomic layer deposition: characterization for photovoltaic applications, Thin Solid Films 617 (2016), https://doi.org/10.1016/j.tsf.2016.03.049.

[31] V. Cimalla, M. Baeumler, L. Kirste, M. Prescher, B. Christian, T. Passow, F. Benkhelifa, F. Bernhardt, G. Eichapfel, M. Himmerlich, S. Krischok, J. Pezoldt. Densification of thin aluminum oxide films by thermal treatments, Mater. Sci. Appl. 5 (2014), https://doi.org/10.4236/msa.2014.58065.

[32] A. Bolshakov, G.M. Pharr, Influences of pileup on the measurement of mechanical properties by load and depth sensing indentation techniques, J. Mater. Res. 13 (4) (1998), https://doi.org/10.1557/JMR.1998.0146.

[33] N. Moharrami, S.J. Bull, A comparison of nanoindentation pile-up in bulk materials and thin films, Thin Solid Films 572 (2014), https://doi.org/10.1016/j.tsf.2014.06.060.

[34] I. Manika, J. Maniks, Effect of substrate hardness and film structure on indentation depth criteria for film hardness testing, J. Phys. D Appl. Phys. 41 (2008), https://doi.org/10.1088/0022-3727/41/7/074010.

[35] C.E. Carlton, P.J. Ferreira, What is behind the inverse Hall-Petch effect in nanocrystalline materials? Acta Mater. 55 (2007) https://doi.org/10.1016/j.actamat.2007.02.021.

[36] Z.C. Cordero, B.E. Knight, C.A. Schuh, Six decades of the Hall-Petch effect – a survey of grain-size strengthening studies on pure metals, Int. Mater. Rev. 61 (8) (2016), https://doi.org/10.1080/09506608.2016.1191808.

[37] H. Kindlund, J. Lu, E. Broitman, I. Petrov, J.E. Greene, J. Birch, L. Hultman, Growth and mechanical properties of 111-oriented $V_{0.5}Mo_{0.5}Nx/Al_2O_3$ (0001) thin films, J. Vac. Sci. Technol. A 36 (2018), 051512, https://doi.org/10.1116/1.5045048.

[38] P. Patsalas, C. Charitidis, S. Logothetidis, C.A. Dimitriadis, O. Valassiades, Combined electrical and mechanical properties of titanium nitride thin films as metallization materials, J. Appl. Phys. 86 (1999) 5296, https://doi.org/10.1063/1.371514.

[39] A.S. Bhattacharyya, S.K. Mishra, S. Mukherjee, Correlation of structure and hardness of rf magnetron sputtered silicon carbonitride films, J. Vac. Sci. Technol. A 28 (2010) 505, https://doi.org/10.1116/1.3420430.

[40] H. Fager, O. Tengstrand, J. Lu, S. Bolz, B. Mesic, W. Kölker, Ch Schiffers, O. Lemmer, J.E. Greene, L. Hultman, I. Petrov, G. Greczynski, Low-temperature growth of dense and hard $Ti_{0.41}Al_{0.51}Ta_{0.08}N$ films via hybrid IPIMS/DC magnetron co-sputtering with synchronized metal-ion irradiation, J. Appl. Phys. 121 (2017) 171902, https://doi.org/10.1063/1.4977818.

[41] J.E. Krzanowski, J.J. Nainaparampil, A.R. Phani, Mechanical and tribological properties of sub- and superstoichiometric Ti-C and Ti-Si-C films deposited by magnetron sputtering-pulsed laser deposition, J. Vac. Sci. Technol. A 21 (2003) 1829, https://doi.org/10.1116/1.1609459.

[42] P. Malinovskis, S. Fritze, l. Riekehr, L. von Fieandt, J. Cedervall, D. Rehnlund, L. Nyholm, E. Lewin, U. Jansson, Synthesis and characterization of multicomponent (CrNbTaTiW)C films for increased hardness and corrosion resistance, Mater. Des. 149 (2018), https://doi.org/10.1016/j.matdes.2018.03.068.

[43] J.J. Roa, P. Sudharshan, W.C. Oliver, L. Llanes, Mapping of mechanical properties at microstructural length scale in WC-Co cemented carbides: assessment of hardness and elastic modulus by means of high speed massive nanoindentation and statistical analysis, Int. J. Refract. Metals Hard Mater. 75 (2018), https://doi.org/10.1016/j.ijrmhm.2018.04.019.

[44] A. Portinha, V. Teixeira, J.O. Carneiro, S.N. Dub, R. Shmegera, C.J. Tavares, Hard ZrO_2/Al_2O_3 nanolaminated PVD coatings evaluated by nanoindentation, Surf. Coat. Technol. 200 (2005), https://doi.org/10.1016/j.surfcoat.2005.02.021.

[45] A. Ito, Y. You, T. Ichikawa, K. Tsuda, T. Goto, Preparation of ZrO2-Al2O3 nanocomposite films by laser chemical vapour deposition, J. Eur. Ceram. Soc. 34 (2014), https://doi.org/10.1016/j.jeurceramsoc.2013.07.025.

[46] G. Balakrishnan, D. Sastikumar, P. Kuppusami, R. Venkatesh Babu, J.I. Song, Microstructural and mechanical properties of ZrO2/Al2O3 nanomultilayer thin films prepared by pulsed laser deposition, Appl. Phys. A (2018), https://doi.org/10.1007/s00339-018-1576-7.

[47] M. Leskelä, J. Niinistö, M. Ritala, Atomic layer deposition. Reference module in materials science and materials engineering, Compr. Mater. Process. 4 (2014), https://doi.org/10.1016/B978-0-08-096532-1.00401-5.

[48] O.M.E. Ylivaara, L. Kilpi, X. Liu, S. Sintonen, S. Ali, M. Laitinen, J. Julin, E. Haimi, T. Sajavaara, H. Lipsanen, S.-P. Hannula, H. Ronkainen, R.L. Puurunen, Aluminium oxide/titanium dioxide nanolaminates grown byatomic layer deposition: growth and mechanical properties, J. Vac. Sci. Technol. A 35 (2017), 01B105, https://doi.org/10.1116/1.49661998.

[49] P. Boryło, k. Lukaszkowicz, M. Szindler, J. Kubacki, K. Balin, M. Basiaga, J. Szewczenko, Structure and properties of Al_2O_3 thin films deposited by ALD process, Vacuum 131 (2016), https://doi.org/10.1016/j.vacuum.2016.07.013.
[50] M.K. Tripp, C. Stampfer, D.C. Miller, T. Helbling, C.F. Hermann, C. Hierold, K. Gall, S.M. George, V.M. Bright, The mechanical properties of atomic layer deposited alumina for use in micro- and nano-electromechanical systems, Sens. Actuators (2006), https://doi.org/10.1016/j.sna.2006.01.029.
[51] K. Tapily, J.E. Jakes, D.S. Stone, P. Shrestha, D. Gu, H. Baumgart, A.A. Elmustafa, Nanoindentation investigation of HfO_2 and Al_2O_3 films grown by atomic layer deposition, J. Electrochem. Soc. 177 (2008), https://doi.org/10.1149/1.2919106.

Institute of Solid State Physics, University of Latvia as the Center of Excellence has received funding from the European Union's Horizon 2020 Framework Programme H2020-WIDESPREAD-01-2016-2017-TeamingPhase2 under grant agreement No. 739508, project CAMART²